Meisoindigo: An Effective Inhibitor of SARS-CoV-2 Main Protease Revealed by Yeast System

Wojciech Grabiński[1], Anna Kicińska[1], Ewa Kosicka[1], Martyna Baranek-Grabińska[1], Ewelina D Hejenkowska[2], Joanna Budzik[1], Paulina Śliska[1], Weronika Śliwińska[1], Andonis Karachitos[1]*

[1]Department of Bioenergetics, Faculty of Biology, Institute of Molecular Biology and Biotechnology, Adam Mickiewicz University, Poznań, Poland.

[2]Department of Pediatrics, University of Virginia, Charlottesville, VA 22903, USA.

*Correspondence: Andonis Karachitos, andonis.karachitos@amu.edu.pl

Abstract

The COVID-19 pandemic caused by SARS-CoV-2 has had a significant impact on global health and economy. Despite the availability of vaccines, their limited accessibility and vaccine hesitancy pose challenges in controlling the spread of the disease. Effective therapeutic strategies, including antiviral drugs, are needed to combat the future spread of new SARS-CoV-2 virus variants. The main protease (M^{pro}) is a critical therapeutic target for COVID-19 medicines, as its inhibition impairs viral replication. However, the use of substances that inhibit M^{pro} may induce selection pressure. Thus, it is vital to monitor viral resistance to known drugs and to develop new drugs. Here we have developed a yeast system for the identification of M^{pro} inhibitors as an alternative to costly and demanding high biosecurity procedures. The system is based on stable expression of M^{pro} and does not require selection media. Yeast can be cultured on a rich carbon source, providing rapid growth and screening results. The designed tool was subsequently used to screen the FDA-Approved Drug Library. Several chemicals with M^{pro} inhibitory properties were identified. We found that meisoindigo not previously known for its potential to inhibit M^{pro}, was highly effective. Our results may promote development of new derivatives with therapeutic properties against SARS-CoV-2 and other beta-coronaviruses.

This work was supported by the research grant of Adam Mickiewicz University, Poznan, Grant Number 6/2020 "Research on COVID-19".

Introduction

The COVID-19 pandemic, caused by the SARS-CoV-2 coronavirus, has had an unprecedented global impact on public health, the economy, and everyday life. Despite the rapid development and deployment of vaccines against SARS-CoV-2, which have proven effective in improving patient outcomes and reducing the transmission of the disease, vaccine availability remains limited in certain regions. Additionally, vaccine hesitancy further complicates the global vaccination efforts. Thus, controlling the spread of the virus and mitigating the impact of COVID-19 worldwide remains the ongoing challenge (Troiano and Nardi, 2021).

In addition, the SARS-CoV-2 virus continues to undergo genetic mutations, particularly in the spike protein (Yuan et al., 2021). These changes may result in reduced immune response, thereby compromising the efficacy of vaccines and previous infections. As a result, there is an urgent need for effective therapeutic strategies to combat the future spread of new variants of the SARS-CoV-2 virus. The development of antiviral substances that directly target viral replication is essential to mitigate the impact of these emerging variants. These drugs can play a critical role in controlling infection, reducing disease severity, and preventing further transmission of SARS-CoV-2.

The main protease (M^{pro}), also named 3-chymotrypsin-like protease (3CLpro), is considered to be the key target for COVID-19 medicines, as it is highly conserved among coronaviruses and plays an important functional role in the viral life cycle. M^{pro} is responsible for the proteolysis of the polyproteins that are translated from viral RNA (Amin et al., 2021). Inhibition of M^{pro} function can disrupt viral replication and has the potential to be highly effective not only against the current pandemic but also against other fatal coronavirus-caused diseases (Ma et al., 2020).

In fact, multiple strategies have been used to screen for effective M^{pro} inhibitors, including drug repurposing, virtual screening and structure-based drug design (Hu et al., 2022). These previous studies resulted in numerous compounds with M^{pro} inhibitory potential, one of which (Paxlovid) is already used in clinics and few others are strong candidates (Hu et al., 2022).

However, it is important to note that the use of drugs targeting M^{pro} can create selection pressure and contribute to the development of resistance (Krishnamoorthy and Fakhro, 2021). Therefore, it is essential to continuously monitor and test for virus resistance to known substances and better understand the mechanisms of enzyme action.

In fact, current studies investigating M^{pro} activity primarily involve *in vitro* assays with isolated protein that allow determination of enzymatic kinetics and functional assays aimed at understanding viral replication in the presence of inhibitors (De Castro et al., 2022; Kitamura

et al., 2022). However, it has recently been proposed to use yeast as a system for the M^{pro} expression (Alalam et al., 2021; Flynn et al., 2022). The yeast system provides an alternative to techniques that measure M^{pro} activity in mammalian cells and addresses their several limitations. It reduces costs associated with the assays and eliminates the need for the high level of biosecurity required when handling samples and performing assays with the SARS-CoV-2.

The use of yeast as an expression system for M^{pro} also offers several other advantages. Yeast cells can be easily cultured and manipulated in the laboratory, allowing for efficient expression of the viral protease. This system allows researchers to study the enzymatic activity and functional effects of M^{pro} in a living cell.

The yeast system, provides rapid access to the effects of potential inhibitors in a cellular context, providing valuable insight into compound entry, stability, and efficacy. This approach offers flexibility, as rapid adjustment of the level of detection and potential modification of the amino acid sequence of M^{pro} to accommodate future mutant variants or enzymes from other betacoronaviruses is straight forward. What is more, the system is cost-effective and maintains a high level of biosafety, making it a promising tool for drug discovery and characterization efforts targeting M^{pro} and related coronaviruses.

In this study, we present a novel yeast system specifically designed for the identification of M^{pro} inhibitors. The key feature of this system is the stable expression of M^{pro}, which is achieved by integrating the Mpro gene into the *GAL1* region of yeast chromosome 2. This integration allows precise control of M^{pro} expression by galactose induction (Peng et al., 2015). Notably, this system does not require the use of selection media and cells can be cultured on a rich carbon source such as sucrose, allowing for rapid growth and accelerated screening results.

In our M^{pro}-expressing strain, we have implemented a unique design for the N-terminal fragment. This design not only reconstitutes the native primary structure of M^{pro}, where the first amino acid is serine, but also releases an N-terminal EGFP fusion protein. The design enhances the enzymatic activity of M^{pro}, resulting in a strong phenotypic effect characterized by toxicity and inhibition of yeast growth. In addition, the fusion of EGFP to M^{pro} provides a sensitive analytical tool for assessing M^{pro} activity, as changes in EGFP fluorescence correlate with changes in M^{pro} activity.

Our yeast system provides a comprehensive and sensitive approach for the identification of M^{pro} inhibitors. The controlled expression of M^{pro}, the phenotypic effects induced by its activity, and the analytical tool of EGFP fusion provide valuable tools for screening and characterizing potential inhibitors. The system was validated with the use of known M^{pro} inhibitors and allowed us to discover a new inhibitor - meisoindigo.

Thus, our yeast-based screening approach provides a valuable tool for the discovery and evaluation of M^{pro} inhibitors, which can ultimately lead to the development of novel drugs and enhance our ability to combat COVID-19 and other related viral infections.

Materials & Methods

Tested compounds

MedChemExpress: FDA-Approved Drug Library Mini (Catalog # HY-L022M). Selleckchem: GC376 (Catalog # S0475). Merck: Tolperisone hydrochloride (Catalog # T3577); Ebselen (Catalog # E3520); Disulfiram (Catalog # PHR1690); Tideglusib (Catalog # SML0339); Carmofur (Catalog # C1494). WuhanChemNorm Biotech: Nirmatrelvir (Catalog # TBW03242).

Construction of plasmids

All the oligonucleotides used are shown in Table S1 (Supplementary file 1). The vectors used for CRISPR/Cas9 were based on the pML104 vector (a gift from John Wyrick; Addgene plasmid # 676380), into which the guide sequences were introduced by site-directed mutagenesis: the pML104-GAL1 vector has a guide sequence 5'-CTCTTAAATTATAGTTGGTT-3' introduced by Q5® Site-Directed Mutagenesis Kit (New England Biolabs) (Hu et al., 2018) while the pML104-PDR1 vector has a guide sequence 5'-CTGGATAAACGTCGCTCCAC-3' introduced by Q5 polymerase PCR (New England Biolabs) and In-Fusion Snap Assembly (Takara) site-directed mutagenesis as described by the manufacturer. Codon-optimized gene encoding EGFP-M^{pro} fusion protein with a linker encoding a cut sequence recognized by M^{pro} (SAVLQ) flanked by sequences downstream (249 nt) and upstream (253 nt) of *GAL1* was synthesized in pBSK(+) Simple-Amp vector by Biomatik (Ontario, Canada). The amino acid sequence of M^{pro} was derived from ORF1a polyprotein (GenBank: UCQ02319.1). pBSK(+)-Mpro(SAVLQ) vector (Figure S1) was used as a template to create an enterokinase-recognized linker variant (D_4K), which had been made using the In-Fusion Snap Assembly (Takara) site-directed mutagenesis. The *mCherry* gene, sourced from the pMitoLoc template vector (Addgene # 58980), was integrated into the pBSK(+)-Mpro(SAVLQ) vector. Supplementary File 1 contains the detailed DNA sequences.

Bacterial and yeast cultures

Bacteria were cultured in LB liquid medium (1 % tryptone, 0.5 % yeast extract, and 1 % sodium chloride) with the addition of ampicillin at a final concentration of 100 µg/ml. Yeast cells were grown in YPD (1 % yeast extract, 2 % peptone, and 2 % D-glucose), when necessary, hygromycin B or G418 was added to the medium at concentrations of 300 or 200 µg/ml, respectively; YPG (1 % yeast extract, 2 % peptone, and 3 % glycerol, pH = 5.5); YPGGal (1 %

yeast extract, 2 % peptone, and 3 % glycerol, pH = 5.5 and 0.5 % galactose); YPSuc (1 % yeast extract, 2 % peptone, and 2 % sucrose); YPSucGal (1 % yeast extract, 2 % peptone, 2 % sucrose, and 0.5 % galactose); SD-ura (0.67 % yeast nitrogen base without amino acids, yeast synthetic drop-out medium supplement without uracil, and 2 % D-glucose) or SDC + 5-FOA (0.67 % yeast nitrogen base without amino acids, yeast complete synthetic drop-out medium supplement, 1 mg / ml 5-fluoroorotic acid and 2 % D-glucose). Agar (2 %) was added to the solid media.

Strains

The bacterial strain NEB® 5-alpha Competent *E. coli* was ordered from New England Biolabs (Catalog # C2987H). Yeast *S. cerevisiae* strains used in this study are derived from the BY4741 and listed in Table S2 (Supplementary file 1). The Δgal1 strain was made by CRISPR/Cas9 using the pML104-GAL1 vector and repair DNA made by hybridizing two complementary oligonucleotides containing a sequence below (35 nt) and above (35 nt) the *GAL1* open reading frame. EGFP-SAVLQ-M^{pro}, EGFP-D4K-M^{pro}, and mCherry strains were obtained by CRISPR/Cas9 technique using repair DNA produced by PCR. The *PDR5* gene was deleted via a KanMX6 deletion cassette. The *PDR1* gene was deleted by CRISPR/Cas9 using the KanMX6 cassette as repair DNA. The *SNQ2* gene was deleted via the HphMX6 cassette. Each application of the CRISPR/Cas9 method involved removal of the pML104 vector from yeast cells by growing the cells in SDC + 5-FOA medium (Laughery and Wyrick, 2019).

Yeast-Based Drug Screening Assay

Yeast after overnight culture on YPG medium were centrifuged and adjusted to OD_{600} = 10. The suspension (0.8 ml) was spread homogeneously with sterile stainless steel beads (3 mm diameter) on a Petri dish (140 mm diameter) containing YPSucGal solid medium. Individual compounds from the chemical library were applied in a volume of 3 µl to sterile filter (6mm diameter). Filter with DMSO was used as a vehicle control. Filters were placed on the agar surface at 10 mm distance (64 filters per plate). Plates were incubated at 28℃ for 48 h and scanned.

Growth and fluorescence assay on liquid medium

The yeast were cultured in a flask on YPG liquid medium. The culture was then inoculated into 1 ml YPSucGal medium in 24-well plates. A drug or DMSO as a vehicle was added to individual wells. The final concentration of DMSO in each well was 1%. The culture plate was incubated using a microplate shaker (PSU-2T, BioSan) at 28℃, 700 rpm. At different time points, the culture was diluted 10x in transparent 96-well plates in 100 µl and OD_{600} was measured. For fluorescence intensity, 100 µl of the undiluted culture was transferred to a 96-well flat bottom plates. EGFP (ex. 485 nm, em. 532 nm) and mCherry (ex. 580 nm, em. 620 nm) fluorescence and OD_{600} were measured with The Spark® multimode microplate reader (TECAN) at RT.

M^{pro} Expression and Purification

BL21(DE3) *E. coli* competent cells were transformed by heat shock with a vector pETM33_Nsp5_Mpro (a gift from Ylva Ivarsson; Addgene plasmid # 156475). Bacteria were cultured on LB medium with kanamycin [50 ug/ml]. When the bacteria reached OD_{600} = 0.6 M^{pro} expression was induced using 0.5 mM IPTG and cultured with shaking for 16 hours at 19℃. Bacteria were centrifuged (10 000g for 6 minutes). The pellet was resuspended in 50 mM Tris-HCl buffer, 150 mM NaCl, pH 8.0 and then sonicated on ice for 80 cycles (15 seconds on, 45 seconds off, amplitude 40%). The lysate was then centrifuged at 18620g for 45 minutes at 4℃. The supernatant was loaded on columns containing Ni-NTA agarose (Qiagen) and incubated at 4℃ on a rotator for 1.5 h (5 RPM). The bed was then washed 3 times with 50 mM Tris-HCl, 150 mM NaCl, pH 8.0 buffer. Pierce™ HRV 3C Protease (Thermo Scientific) was added to facilitate elution and the digestion was performed overnight at 4℃. After elution, the protein was concentrated using Amicon® (Merck) and stored in 50 mM Tris-HCl, 1mM EDTA buffer, pH 7.3 in -20℃.

Measurement of M^{pro} inhibition

The inhibition of SARS-CoV-2 M^{pro} *in vitro* enzymatic activity was measured as previously described (Liu et al., 2022). Briefly, the enzyme activity was measured by a continuous kinetic assay, with the substrate Mca–AVLQ↓SGFR-K(Dnp)K (Merck). The mixture of 2 µM SARS-CoV-2 M^{pro} with 50 µM inhibitors or DMSO (vehicle control) was incubated for 20 min in 50 mM Tris-HCl (pH 7.3), 1 mM EDTA at room temperature. The reaction was then initiated by the addition of 20 µM substrate. Fluorescence intensity (Excitation 320 nm, Emission 405 nm) was monitored with The Spark® multimode microplate reader (TECAN) at 30℃.

Statistics

Statistical analysis was performed using GraphPad Prism software version 9.5.1 (GraphPad Software, San Diego, CA, USA). Data are presented as mean ± standard deviation (SD) or Standard Error of the Mean (S.E.M.) from at least three independent experiments. Statistical significance was assessed by Welch and Brown-Forsythe one-way analysis of variance (ANOVA) for comparing three or more groups, or Student's t-test for comparing two groups. P values less than 0.05 were considered statistically significant.

Results & Discussion

The yeast system

During the development of our yeast expression system, our primary goal was to establish stable expression of the target protein, specifically the M^{pro}, which was intentionally designed to be toxic to cells. We recognized that the use of classical vector-based expression systems would require the implementation of special selection pressure conditions, such as minimal media, which cannot adequately support robust culture growth. To overcome this challenge, we chose a technique that allowed us to integrate the M^{pro} expressing gene directly into the yeast genome (Figure 1A). The CRISPR/Cas9 system we developed allowed us to integrate the gene encoding M^{pro} into the yeast chromosome. This system consists of a vector containing Cas9, sgRNA, and a separate vector containing the repair DNA. An important advantage of our system was its ability to facilitate rapid modification and redesign of the entire yeast system, allowing us to efficiently express mutant variants of M^{pro}.

By integrating the *M^{pro}* gene into the *GAL1* locus, we achieved precise control over its expression by simply adding galactose to the growth medium. However, it's important to note that the gene knock-in procedure we employed resulted in the removal of the *GAL1* gene from the yeast strain. As a result, the yeast strain no longer possesses the ability to consume galactose as a carbon source. This characteristic allows us to supply small concentrations of galactose in the medium to effectively induce M^{pro} expression. In the context of drug screening, the yeast strain we constructed faces limitations regarding the use of galactose as a carbon source (Bhat et al., 1990). In addition, glucose-rich medium cannot be used in due to the phenomenon of catabolic repression. High glucose concentrations inhibit the induction of gene expression by galactose (Gancedo, 1998). Consequently, the *GAL1* promoter remains inactive in the absence of galactose or in the presence of repressive carbon sources such as glucose, resulting in minimal or no gene expression.

The next goal in designing the yeast system for drug screening was to eliminate yeast multidrug resistance, which could potentially interfere with screening results. To accomplish this, we chose to delete three specific genes: *PDR5* and *SNQ2*, which encode multidrug resistance transporters, and *PDR1*, which functions as a transcription factor that regulates pleiotropic drug response (Decottignies et al., 1998). By removing these genes from the yeast genome, we aimed to minimize any confounding effects of multidrug resistance and improve the accuracy of our drug screening results. After deletion of the three targeted genes, we observed a significant change in the phenotype of the yeast strain expressing M^{pro} - EGFP-SAVLQ-Mpro Δpdr5, Δsnq2, Δpdr1. However, this change rendered the screening process

infeasible. Interestingly, the mutant strains (EGFP-SAVLQ-Mpro Δpdr5, Δsnq2 and EGFP-SAVLQ-Mpro Δpdr5, Δsnq2, Δpdr1) showed significantly enhanced growth capabilities compared to the original strain with only one *PDR5* gene deleted - EGFP-SAVLQ-Mpro (see Figure S2). This unexpected improvement in the growth ability of the mutants underscored the complex interplay between multidrug resistance and yeast physiological responses. While it posed a challenge to our drug screening efforts, it also shed light on the intricate mechanisms underlying drug resistance in yeast. The observed phenomenon of enhanced growth in our mutant strains, despite the deletion of the three selected genes, remains unexplained. Interestingly, we came across a previously reported yeast system in which M^{pro} is expressed in a strain lacking not only *PDR1* and *SNQ2*, but also *PDR3*. Surprisingly, this strain exhibited significantly weaker cytotoxicity induced by M^{pro} expression compared to our variant that had only a *PDR5* deletion (Alalam et al., 2021). The different results observed between the two systems highlight the complexity of the factors influencing M^{pro} expression-induced cytotoxicity. These results underscore the importance of further investigations to elucidate the underlying mechanisms. In our particular case, the specific culture conditions and yeast phenotype required the use of only the *pdr5*Δ mutant to achieve the desired and optimal result in terms of drug screening.

One of the primary challenges we faced was selecting the optimal culture conditions to accelerate the drug screening process. To achieve this, our initial approach was to test drugs on a glycerol supplemented medium. Although we observed a significant change in the yeast phenotype upon induction of M^{pro} expression (Figure 2C), our attempts to screen the drug library using glycerol as a non-fermentable carbon source were unsuccessful. None of the drugs showed any effect on the yeast phenotype (see Figure S3). In addition, the drug screening process was about a weeklong, which was too long for our needs. Previous studies have shown that galactose can strongly activate *GAL1* gene when yeast are grown on glycerol media. However, glycerol itself is a weak carbon source, which may have contributed to the limited success of our drug screening approach (Hashimoto et al., 1983). To address the limitations encountered during the drug screening process, the same authors proposed an alternative carbon source: sucrose (Hashimoto et al., 1983). This choice offered several advantages, including significantly enhanced cell growth compared to glycerol and minimal catabolic repression. We found that under optimized growth conditions, yeast cells exhibited significant cytotoxicity following the induction of M^{pro} with galactose. This cytotoxic effect, believed to be a result of the overexpression of M^{pro}, led to a clear reduction in the growth rates of the yeast (Figure 1B). By using sucrose as the carbon source in our system, the drug screening could be performed in a much shorter time interval. Remarkably, screening results

were visible after only 24 hours, and the entire experiment was completed within a maximum of 48 hours. This timeline greatly accelerated the drug discovery process (Figure 1C).

A notable feature of our yeast system is the fusion of EGFP to the N-terminus of M^{pro}. This fusion allows autocatalytic cleavage by M^{pro} itself (as shown in Figure 2A). As a result of this cleavage, M^{pro} becomes fully active and subsequently inhibits yeast cell growth. The autocatalytic cleavage of M^{pro} is reminiscent of the process by which M^{pro} of the SARS-CoV virus is formed. In the case of viral genomic RNA, the polyproteins pp1a pp1ab are expressed and undergo autocatalytic cleavage to generate functional M^{pro} (V'kovski et al., 2021). However, the enzymatic activity of M^{pro} is inhibited by the presence of additional N- and C-terminal amino acids (Xue et al., 2007). We introduced a modified gene with a D_4K linker between EGFP and M^{pro} to serve as a control strain without cytotoxicity upon M^{pro} expression. This linker prevents the enzymatic activity of M^{pro}. In contrast, the EGFP-SAVLQ-Mpro strain contains a sequence that is recognized and cleaved by M^{pro}. As shown in Figure 2B, there is a marked difference in fluorescence between the EGFP-SAVLQ-Mpro and EGFP-D_4K-Mpro strains. The EGFP-D_4K-Mpro strain, which lacks M^{pro} cleavage site, exhibits significantly higher green fluorescence compared to the EGFP-SAVLQ-Mpro strain. Consistent with this observation, the yeast phenotype (as shown in Figure 2C) confirms that the EGFP-D_4K-Mpro strain does not exhibit growth inhibition, further supporting the role of the D_4K linker in preventing M^{pro}-induced cytotoxicity.

Screening the drug library

As mentioned above, the yeast system we developed is characterized by growth limitations induced by M^{pro} expression (Figure 1B). The presence of M^{pro} exerts a cytotoxic effect on the yeast cells, resulting in inhibited growth and compromised viability. This growth limitation serves as a key feature of our system, allowing us to evaluate the impact of various compounds, including potential M^{pro} inhibitors, on yeast growth under these challenging conditions (Figure 1C).

Prior to screening over 1,800 FDA-approved compounds from our library, we conducted an initial investigation to assess the system's ability to effectively identify M^{pro} inhibitors. To accomplish this, we used GC376, a control compound known for its activity against the 3CLpro of several coronaviruses, including SARS-CoV and SARS-CoV-2 (Shi et al., 2021). Our goal was to evaluate whether our system could accurately select M^{pro} inhibitors.

The use of GC376 in our system yielded a positive result. The yeast strains expressing M^{pro} showed increased growth specifically around the filter containing the drug (Figure 3A,

induced). This finding validated the efficacy of GC376 as an M^{pro} inhibitor in our system. However, during the screening phase, we also observed that certain drugs, such as ebselen, which had shown promise as an M^{pro} inhibitor (Jin et al., 2020), had no detectable effect on our system (Figure 3B). This lack of response was attributed to the general toxicity of ebselen, which affected overall yeast growth rather than specifically targeting M^{pro}.

A comprehensive search of the drug library led to the identification of several candidates with potential inhibitory effects on M^{pro}: 9-aminoacridine, bedaquiline, berberine, ciclopirox, ethacridine, ixazomib, meisoindigo, menadione, pomalidomide and tedizolid (see Supplementary file 2). Notably, two of these identified drugs (ixazomib and meisoindigo) induced significant changes in the phenotype of the yeast strain expressing M^{pro}, as shown in Figure 3B and C. It is worth mentioning that some of these drugs have been previously reported in the literature, highlighting their potential relevance in inhibiting M^{pro} activity and supporting their candidacy as therapeutic agents. Two of the drugs identified, ixazomib and pomalidomide, have been suggested as a potential M^{pro} inhibitor in in silico studies (Elzupir, 2020; Vázquez-Mendoza et al., 2022). The identification of ixazomib in our drug library screening, combined with previous in silico evidence, suggests its potential as an M^{pro} inhibitor. Ethacridine, another drug identified in our screening, has shown inhibitory effects on SARS-CoV-2 virus particles (Li et al., 2021). The inhibitory effects observed in previous studies provide encouraging evidence for the potential of ethacridine as a therapeutic agent against SARS-CoV-2.

Despite the initial promising screening results, ixazomib, ethacridine and other drugs were found to be only slightly effective as an inhibitor in subsequent steps on liquid medium as shown in Figure 4C. However, it is important to note that the possibility that ixazomib possesses M^{pro} inhibitory activity cannot be completely excluded. In the downstream steps of the work, ixazomib will serve as a control, representing a weak inhibitor compared to GC376, as shown in Figure 4D.

In addition to drugs that have been previously studied and reported, our work also identified several drugs that have not previously been associated with M^{pro} inhibition. These drugs represent novel findings and were identified as potential M^{pro} inhibitors for the first time in our screening. Their identification in this study highlights their previously unexplored potential in targeting M^{pro} and suggests avenues for further investigation to determine their efficacy and mechanism of action.

Of particular importance is the drug meisoindigo (for the chemical structure, see Figure S4), a derivative of indigo naturalis, an active compound in a Chinese anti-leukemia medicine with proven efficacy in the treatment of chronic myelogenous leukemia (CML) (Lee et al., 2010; Ye

et al., 2019). In our studies, the performance of meisoindigo was particularly noteworthy (Figure 4B). At a concentration of 30 µM and after 24 hours, the optical density (OD) of yeast culture was 0.48 ± 0.018 vs. 0.074 ± 0.004 in control culture (DMSO). Interestingly, at a higher concentration of 100 µM, meisoindigo did not protect yeast against M^{pro} toxicity that well (OD = 0.30 ± 0.023). This reduced efficacy at higher concentrations underscores the challenges posed by meisoindigo's solubility properties in water. Meisoindigo, a second-generation derivative of indirubin, exhibits enhanced water solubility compared to its precursor (Ye et al., 2019). While this enhanced solubility facilitates its application in various mediums, it also seems to limit its efficacy at higher concentrations.

In contrast, nirmatrelvir, a component of the FDA-approved drug Paxlovid used in the treatment of COVID-19, demonstrated a yeast growth mean value of 0.37 ± 0.005 at 24 hours for a concentration of 30 µM (Figure 4A). At the 100 µM concentration, nirmatrelvir's mean value was significantly higher, 0.58 ± 0.015. The proximity of these results, especially at the 30 µM concentration, is striking, especially when considering the different chemical properties of the two compounds.

When comparing the effects on growth, both compounds show significant potential at the 30 µM concentration. However, at 100 µM, nirmatrelvir appears to maintain its efficacy better than meisoindigo. This is particularly significant for meisoindigo, given its solubility challenges.

The solubility of meisoindigo in water, while presenting certain limitations, also offers intriguing possibilities for further research. Its enhanced solubility compared to indirubin suggests that there might be ways to further optimize its formulation for even better results. Enhancing its solubility or finding ways to stabilize it at higher concentrations could potentially amplify its efficacy, making it an even more potent agent in future applications.

Indirubin compounds, including Indigo, have been previously suggested as potential inhibitors of the SARS coronavirus M^{pro} (Khalifa et al., 2021; Lin et al., 2005). Therefore, the inclusion of meisoindigo, a derivative of indigo naturalis, in our assays is consistent with existing knowledge regarding the potential anti-SARS coronavirus activity of indirubin compounds. The impressive results observed with meisoindigo further support its potential as an M^{pro} inhibitor and warrant further investigation for its therapeutic applications, particularly in the context of COVID-19.

In vitro M^{pro} inhibition

The outcomes of our *in vivo* tests were confirmed through *in vitro* studies of M^{pro} inhibition using 50 µM meisoindigo. Enzymatic activity of purified M^{pro} protein was studied. As shown in

Figure 5A, meisoindigo showed significant inhibitory activity towards M^{pro}. This is in stark contrast to ixazomib, which showed significantly less efficacy. The comparison with GC376, a well-established M^{pro} inhibitor, is shown in Figure 5B. Meisoindigo inhibitory potential reaches 78.8 ± 35 % of GC376. As this potential is further underscored by *in vivo* assay in yeast cells, our results suggest that meisoindigo may be a strong candidate for M^{pro} inhibition in a biologically relevant context.

EGFP fluorescence assay

As mentioned above, the primary reason for designing our system so that M^{pro} would be expressed as a fusion protein with the EGFP at the N-terminus was to ensure that M^{pro} is active and would autocatalytically cleave upon recognition of the linker sequence (SAVLQ). The second reason for choosing this approach was the ability to monitor gene expression in a real time, as indicated by green fluorescence. This method provides immediate visual feedback on the activity of the *GAL1* promoter.

Based on the notable difference observed in the growth of EGFP-SAVLQ-Mpro and EGFP-D4K-Mpro strains (Figure 2C), which was correlated with a significant difference in EGFP fluorescence levels (Figure 2B and 6A), we decided to investigate whether these fluorescence levels could serve as an additional bio-indicator of the efficacy of M^{pro} inhibitors. During our experiment, the fluorescence intensity of yeast culture in the presence of different drugs was evaluated. Within just 3 hours of drug exposure the fluorescence was significantly increased by all of the studied inhibitors, and, with the respective recorded values of 4.66 ± 0.13 x 10^4 (10 µM ixazomib), 4.89 ± 0,19 x 10^4 (1 µM meisoindigo), 5.02 ± 0.12 x 10^4 (500 µM GC376), and· 4.49 ± 0.05 x 10^4 (100 µM nirmatrelvir), compared to 4.34 ± 0.12 x 10^4 for control (DMSO) (Figure 6B). By the 24-hour mark, the differences were even more pronounced reaching 2.79 ± 0,04 x 10^4 (1 µM meisoindigo) and 5.17 ± 0.19 x 10^4 (500 µM GC376) in comparison to 1.79 ± 0.03 x 10^4 for control (DMSO), Figure 6C.

The use of GFP as a biosensor for cytotoxic compounds has been previously recognized. Transgenic *Leishmania infantum* promastigotes that continuously express green fluorescent protein (GFP) were used to monitor the effects of antileishmanial compounds (Kamau et al., 2001). The GFP-based assay served as a reliable measure of the inhibitory effects of the drugs on protein expression, providing a dynamic representation of how the leishmanial promastigotes responded to the compounds being tested. A prominent example of these assays is the GreenScreen genotoxicity assay, which has the ability to simultaneously measure both toxicity and genotoxicity in yeast (Cahill et al., 2004). The first description of the use of GFP-expressing mammalian cells for cytotoxic screening involved the use of the

inducible Tet-On system to drive the expression of EGFP in HeLa cells (Sandman et al., 1999). This was used to assess the cytotoxicity of cisplatin. When the HeLa cells with inducible GFP expression were treated with cisplatin and other platinum complexes, a strong correlation was observed between the GFP fluorescence decline and cytotoxicity.

Similarly, in our system, the decrease in EGFP fluorescence intensity due to the presence of active M^{pro} serves as an indicator of the cytotoxicity of the expressed enzyme. However, as we have also shown in Figure S5, the fluorescence level of the protein can be reduced under conditions where the cytotoxicity of the enzyme itself is absent, which could be due to the general cytotoxicity of the test drug.

Consequently, we found that meisoindigo, an anticancer drug, could exhibit toxicity at higher concentrations (especially those above 3 µM), leading to a decrease in the fluorescence of the fluorescent protein (EGFP in fusion with inactive M^{pro} or mCherry alone). Furthermore, the toxicity of meisoindigo reduced yeast growth and was strongly dependent on the genetic background. For example, strains with deletions of the *pdr5*Δ, *pdr1*Δ, and *snq2*Δ genes were understandably much more sensitive to 3 µM meisoindigo than the *pdr5*Δ variant (Figure S6). Interestingly, the toxicity was not associated with the *GAL1* promoter, as it also occurred on medium (YPD) that causes *GAL1* repression.

Conclusions

A yeast system characterized by growth restriction induced by M^{pro} expression was developed and used to evaluate the effects of various compounds, including potential M^{pro} inhibitors. An initial screen using the known M^{pro} inhibitor GC376 validated the system's ability to identify M^{pro} inhibitors. A comprehensive search of a drug library identified several candidates with potential inhibitory effects on M^{pro}, including ixazomib and ethacridine, which had been suggested as potential Mpro inhibitors in previous studies. However, these drugs were found to be ineffective in subsequent liquid medium assays. The study also identified several drugs not previously associated with M^{pro} inhibition, including meisoindigo, a derivative of indigo, which showed significant inhibitory activity against M^{pro} in both *in vivo* and *in vitro* assays. In the study, an EGFP fusion was used to track M^{pro} protein activity and gene expression, serving as a potential indicator for M^{pro} inhibitor efficacy. The decrease in EGFP intensity signaled the cytotoxicity of the active M^{pro} enzyme, although it could also reflect the cytotoxicity of the test drug.

The observed increase in fluorescence intensity was associated with inhibition of M^{pro} activity, while ensuring that the drug concentration did not induce cytotoxicity to the cell. This makes the developed system highly valuable for screening potential inhibitors, both at the level of the survival assay and by a highly sensitive method based on EGFP fluorescence. Using these methods, meisoindigo was identified as a potent M^{pro} inhibitor. The discovery of this new compound with potential M^{pro} inhibitory activity could open new avenues of research, including the creation of new derivatives that could potentially serve as drugs for SARS-CoV-2 and other coronavirus infections.

Figures

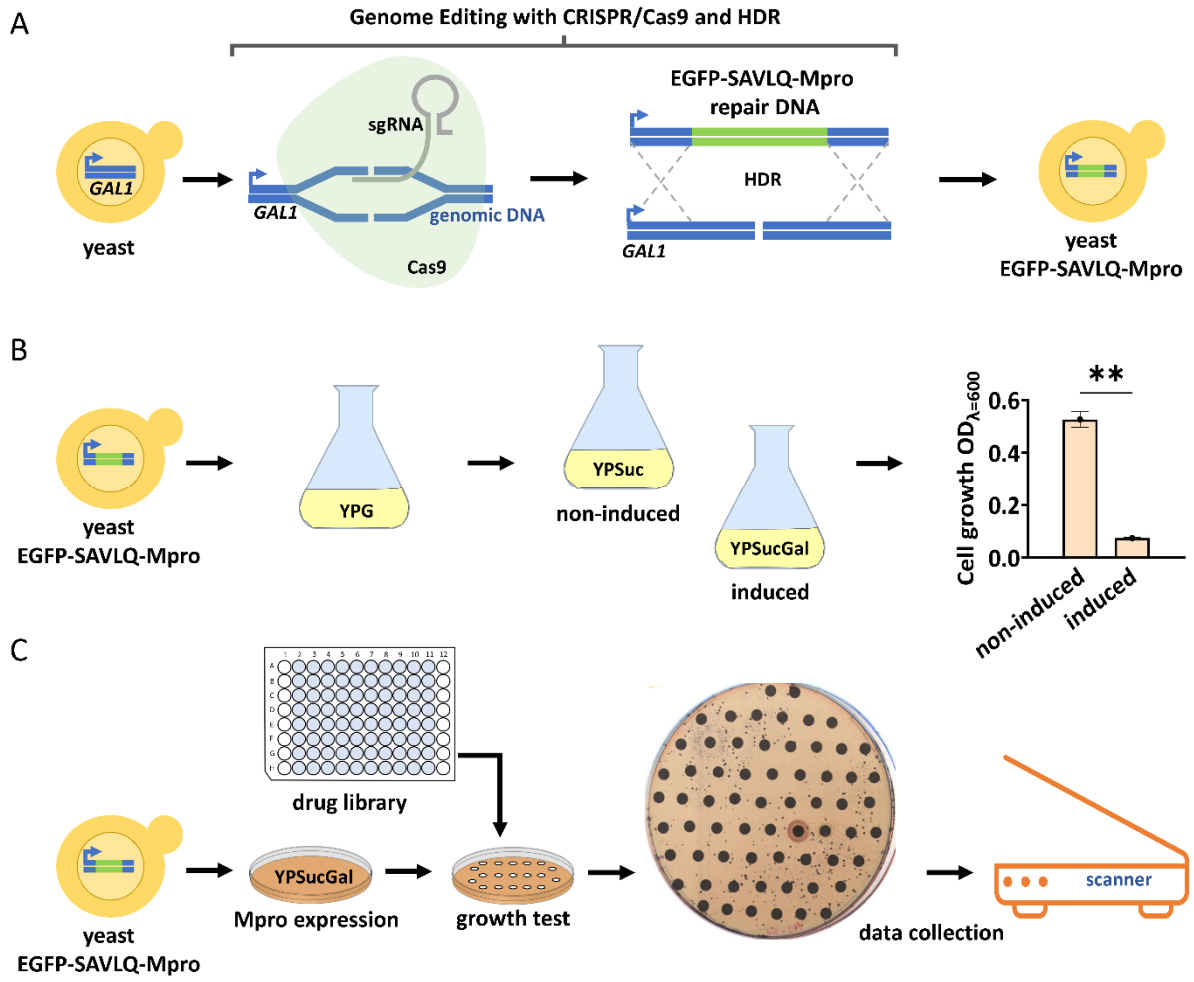

Figure 1. The yeast system designed for the identification of M^{pro} inhibitors.

A) Illustration showing the method of EGFP-SAVLQ-Mpro encoding gene integration into the yeast genome. The CRIPSR/Cas9 system recognizes a specific site within *GAL1* which causes the double strand break. By flanking homology to regions downstream and upstream of *GAL1* within the repair DNA, homology-directed repair (HDR) and integration of a new gene at the *GAL1* site takes place. By using this technique, the EGFP-SAVLQ-Mpro coding gene is under the control of the GAL1 promoter. **B)** Differences in yeast culture growth depending on M^{pro} expression. The asterisks (**) indicate that the p-value is less than 0.01 (n=3). Error bars represent the Standard Deviation (SD). **C)** Utilizing a yeast system to screen a drug library for M^{pro} inhibitors. Yeast culture is spread homogeneously on a plate with solid medium, which leads to the induction of M^{pro} expression and induces growth suppression. Application of filters containing drugs from the library allows high-throughput screening of potential M^{pro} inhibitors based on difference in culture growth.

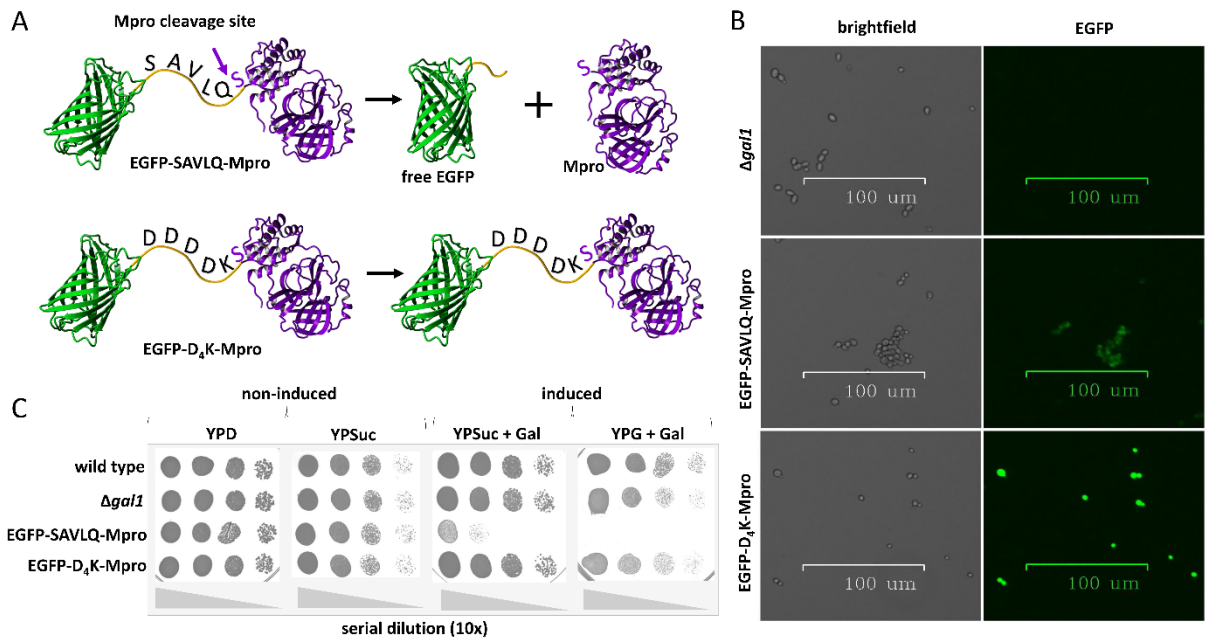

Figure 2. EGFP-M^{pro} linkers and their effect on M^{pro} function and expression.

A) An illustration showing the structure of the fusion proteins being expressed in the yeast used in this work. EGFP-SAVLQ-Mpro contains EGFP at the N-terminus, followed by a sequence (SAVLQ) that is recognized and autocatalytically cleaved by M^{pro}. As a result, EGFP is released and M^{pro} reconstitutes native structure is fully active. Replacing the sequence recognized by M^{pro} with the sequence recognized by enterokinase (D_4K) provides the same linker length but prevents M^{pro} from cleaving off the N-terminal EGFP in vivo, and in consequence inhibits Mpro's enzymatic activity. YASARA was used to visualize and render the final figure of the fused EGFP (PDB: 6YLQ) and M^{pro} (PDB: 7QT5) protein structures. **B)** Differences in green fluorescence of Δgal1 (no EGFP) and EGFP-SAVLQ-Mpro or EGFP- D_4K-Mpro (EGFP expression) strains. The images were made with the ZOE Fluorescent Cell Imager (BioRad) **C)** Differences in the growth of cultures of different strains depending on the medium used and the type of linker used between EGFP and M^{pro}.

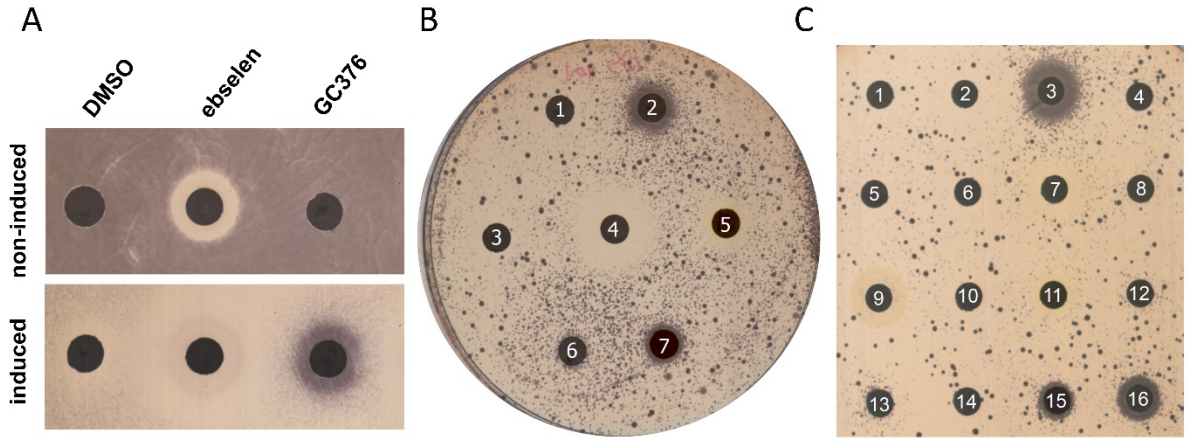

Figure 3. Effect of M^{pro} expression and potential inhibitors on yeast growth.

A) Effects of a potential M^{pro} inhibitor (ebselen) and a known 3Cl protease inhibitor (GC376) on the growth of Mpro-expressing yeast. Limited growth of cultures with non-induced M^{pro} expression may indicate general cytotoxicity of the drug within its diffusion circle (ebselen) while increased growth of cultures with induced M^{pro} expression suggests an inhibitory effect on M^{pro} activity (GC376). **B)** The effect of the drugs selected in this work after the first screening on the growth of the yeast system for induced culture; 1 – DMSO or 10 mM drug: 2 – GC376, 3 – bedaquiline, 4 – berberine, 5 – ethacridine, 6 – ixazomib, 7- meisoindigo. **C)** The effect of selected drugs on the growth of yeast with M^{pro} expression depending on the drug concentration; 1 – empty filter, 2 – DMSO, 3 – 50 μM GC376, 4 – 5 μM GC376, 5 – 10 μM bedaquiline, 6 – 1 μM bedaquiline, 7 – 10 μM berberine, 8 – 1 μM berberine, 9 – 10 μM ciclopirox, 10 – 1 μM ciclopirox, 11 – 10 μM ethacridine, 12 – 1 μM ethacridine, 13 – 10 μM ixazomib, 14 – 1 μM ixazomib, 15 – 10 μM meisoindigo, 16 – 1 μM meisoindigo.

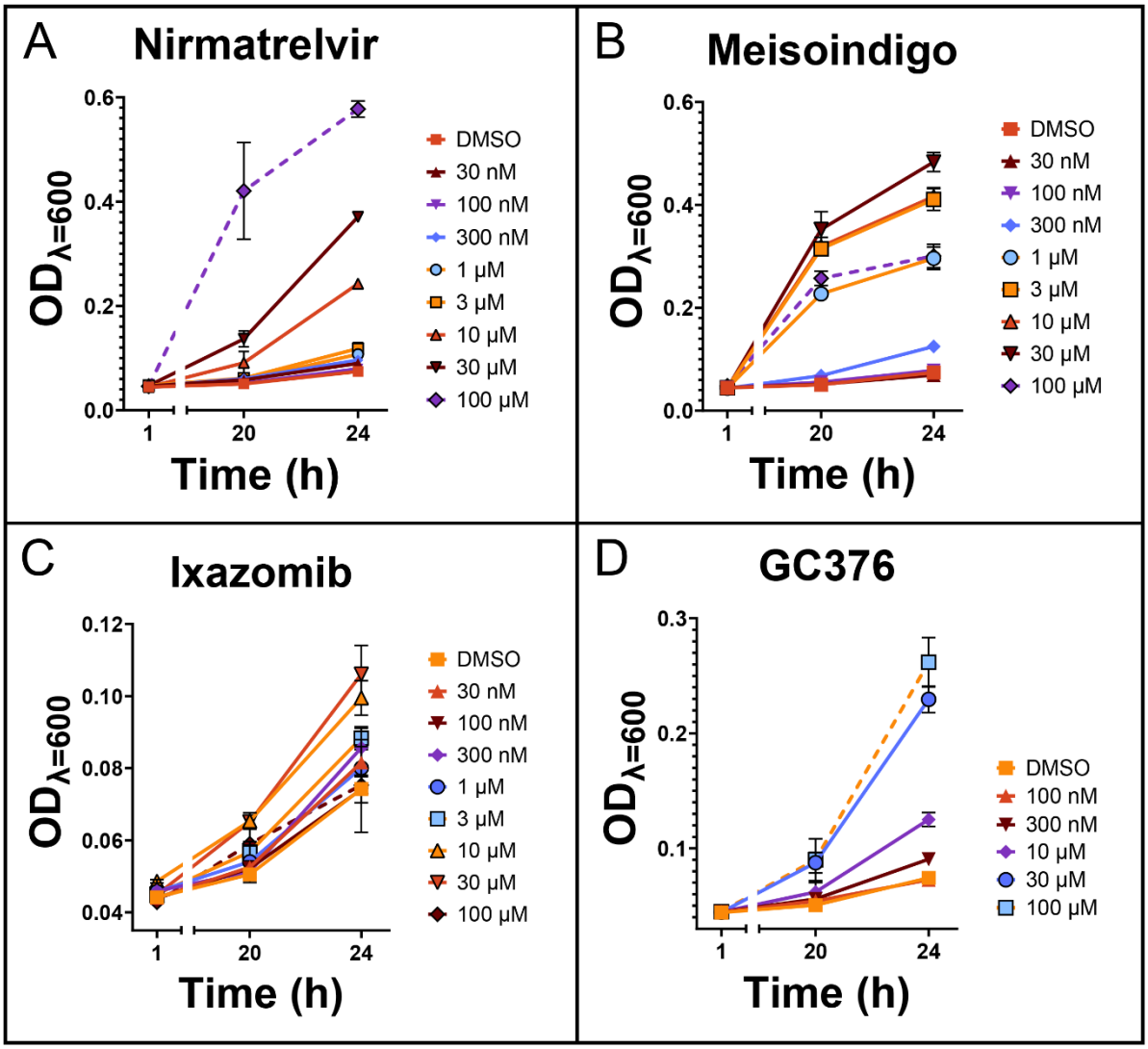

Figure 4. Drug concentration-dependent effects on the growth of M^{pro}-expressing yeast.

The red line in the graph represents a control group that has not been treated with the drug. The error bars on the graph represent the Standard Deviation (SD) for a total of three measurements (n = 3). In order to effectively illustrate the effect of the drug, the scale of the Y-axis varies between the different graphs.

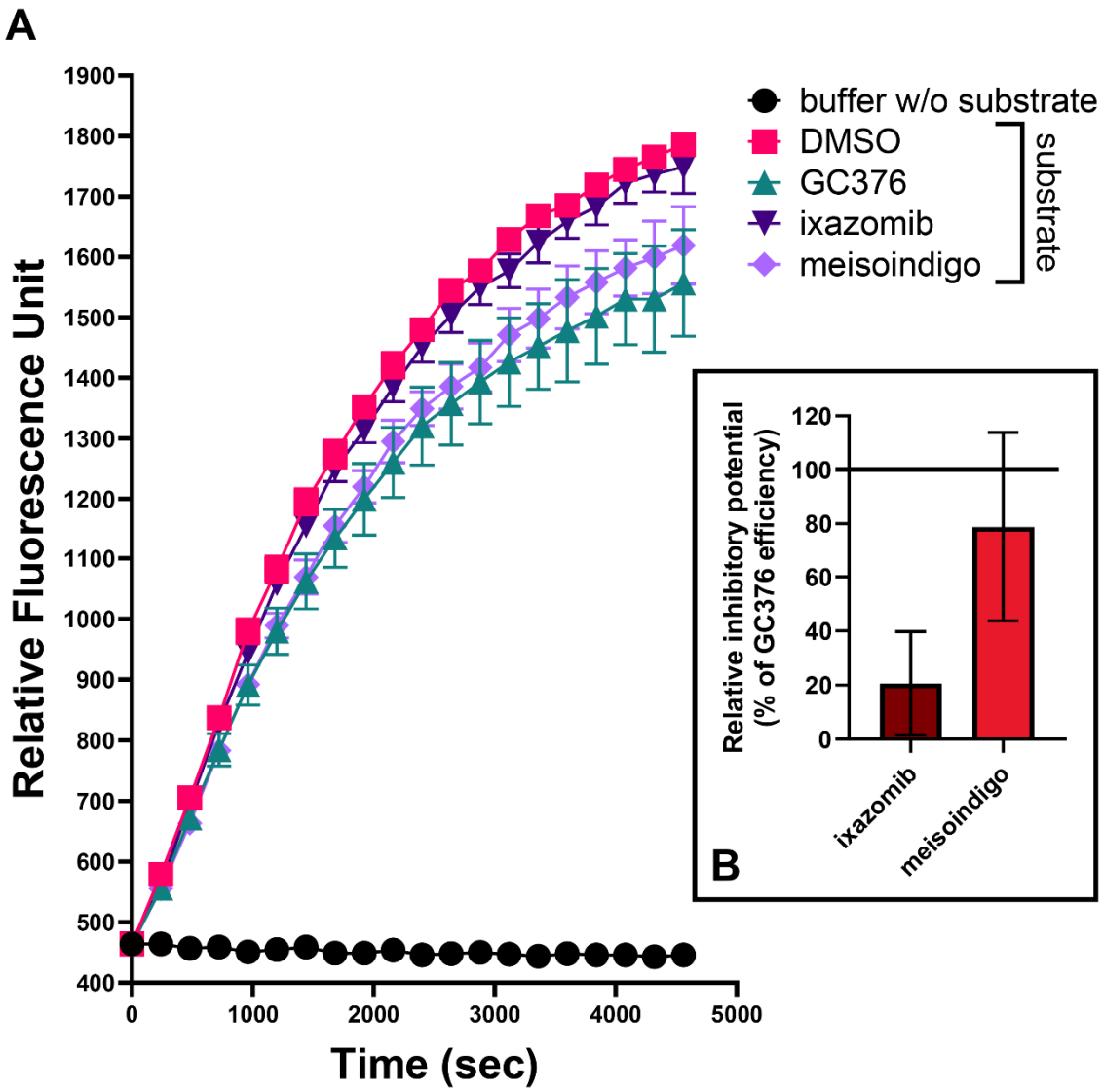

Figure 5. Evaluation of drugs efficacy on the proteolytic activity of M^{pro}.

(A) Results of enzyme assay using FRET-based substrate Mca-AVLQ↓SGFR-K(Dnp)K. The graph shows the changes in M^{pro} protease activity under the influence of different drugs, each at a concentration of 50 µM. The changes in fluorescence intensity, indicative of substrate cleavage, provide insight into the inhibitory effects of the drugs on M^{pro} activity. Error bars represent the standard error of the mean (S.E.M.) of three measurements (n = 3). **(B)** A calculated parameter that indicates the potential of the drugs ixazomib and meisoindigo to inhibit M^{pro} in comparison with the activity of the well-established drug GC376.

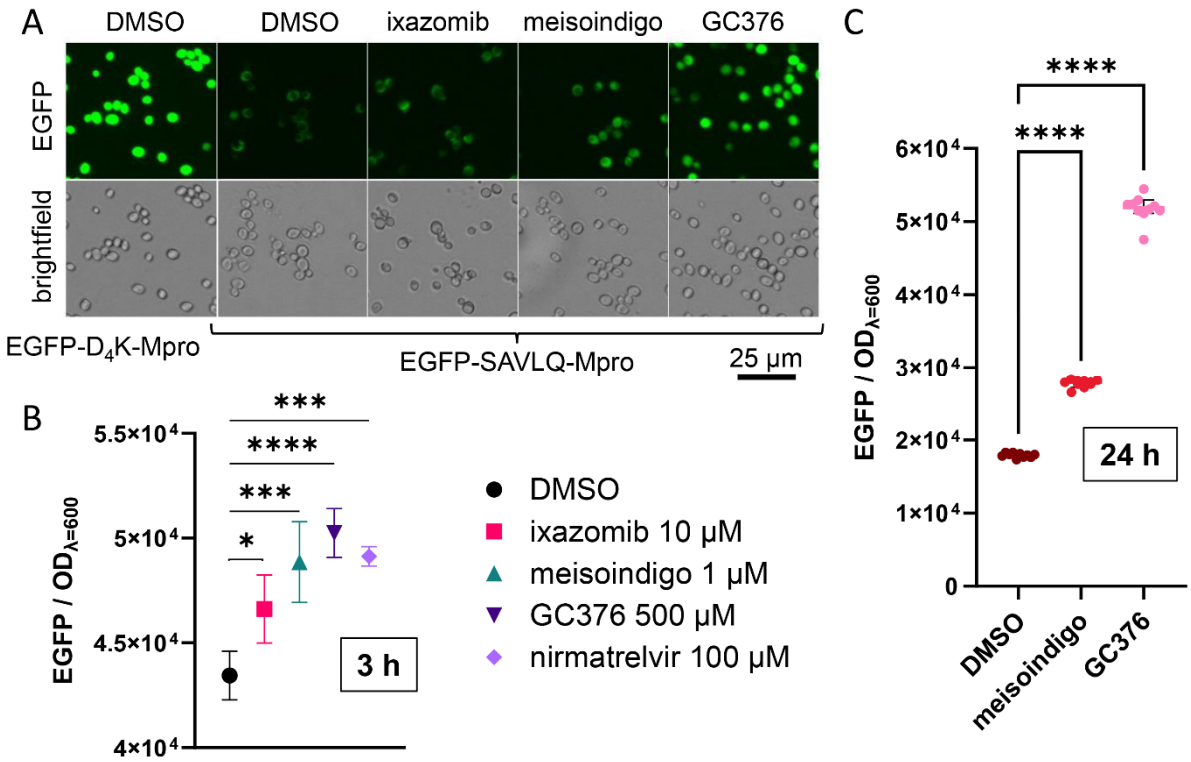

Figure 6. Quantitative analysis of green fluorescence of EGFP-SAVLQ-Mpro cells.

(A) Microscopic images of EGFP-SAVLQ-Mpro yeast cells treated with various drugs, including an additional control of the EGFP-D4K-Mpro strain. **(B)** A quantitative analysis of green fluorescence levels in EGFP-SAVLQ-Mpro cells 3 hours after induction, with (*) indicating $p < 0.05$, (***) indicating $p < 0.001$, and (****) indicating $p < 0.0001$ based on $n = 3$ measurements. **(C)** The fluorescence levels 24 hours post-induction, with (****) indicating a p-value less than 0.0001 for $n = 10$ measurements. Across all sections, the drug concentrations are consistent and are as indicated in B. Error bars represent Standard Deviation (SD), and images were captured using the ZOE Fluorescent Cell Imager (BioRad).

Literature

Alalam, H., Sigurdardóttir, S., Bourgard, C., Tiukova, I., King, R.D., Grøtli, M., Sunnerhagen, P., 2021. A Genetic Trap in Yeast for Inhibitors of SARS-CoV-2 Main Protease. mSystems 6, e01087-21. https://doi.org/10.1128/mSystems.01087-21

Amin, Sk.A., Banerjee, S., Ghosh, K., Gayen, S., Jha, T., 2021. Protease targeted COVID-19 drug discovery and its challenges: Insight into viral main protease (Mpro) and papain-like protease (PLpro) inhibitors. Bioorg. Med. Chem. 29, 115860. https://doi.org/10.1016/j.bmc.2020.115860

Bhat, P.J., Oh, D., Hopper, J.E., 1990. Analysis of the Gal3 Signal Transduction Pathway Activating Gal4 Protein-Dependent Transcription in Saccharomyces Cerevisiae. Genetics 125, 281–291.

Cahill, P.A., Knight, A.W., Billinton, N., Barker, M.G., Walsh, L., Keenan, P.O., Williams, C.V., Tweats, D.J., Walmsley, R.M., 2004. The GreenScreen genotoxicity assay: a screening validation programme. Mutagenesis 19, 105–119. https://doi.org/10.1093/mutage/geh015

De Castro, S., Stevaert, A., Maldonado, M., Delpal, A., Vandeput, J., Van Loy, B., Eydoux, C., Guillemot, J.-C., Decroly, E., Gago, F., Canard, B., Camarasa, M.-J., Velázquez, S., Naesens, L., 2022. A Versatile Class of 1,4,4-Trisubstituted Piperidines Block Coronavirus Replication In Vitro. Pharm. Basel Switz. 15, 1021. https://doi.org/10.3390/ph15081021

Decottignies, A., Grant, A.M., Nichols, J.W., de Wet, H., McIntosh, D.B., Goffeau, A., 1998. ATPase and multidrug transport activities of the overexpressed yeast ABC protein Yor1p. J. Biol. Chem. 273, 12612–12622. https://doi.org/10.1074/jbc.273.20.12612

Elzupir, A.O., 2020. Inhibition of SARS-CoV-2 main protease 3CLpro by means of α-ketoamide and pyridone-containing pharmaceuticals using in silico molecular docking. J. Mol. Struct. 1222, 128878. https://doi.org/10.1016/j.molstruc.2020.128878

Flynn, J.M., Samant, N., Schneider-Nachum, G., Barkan, D.T., Yilmaz, N.K., Schiffer, C.A., Moquin, S.A., Dovala, D., Bolon, D.N.A., 2022. Comprehensive fitness landscape of SARS-CoV-2 Mpro reveals insights into viral resistance mechanisms. eLife 11, e77433. https://doi.org/10.7554/eLife.77433

Gancedo, J.M., 1998. Yeast carbon catabolite repression. Microbiol. Mol. Biol. Rev. MMBR 62, 334–361. https://doi.org/10.1128/MMBR.62.2.334-361.1998

Hashimoto, H., Kikuchi, Y., Nogi, Y., Fukasawa, T., 1983. Regulation of expression of the galactose gene cluster in Saccharomyces cerevisiae. Isolation and characterization of the regulatory gene GAL4. Mol. Gen. Genet. MGG 191, 31–38. https://doi.org/10.1007/BF00330886

Hu, G., Luo, S., Rao, H., Cheng, H., Gan, X., 2018. A Simple PCR-based Strategy for the Introduction of Point Mutations in the Yeast Saccharomyces cerevisiae via CRISPR/Cas9. Biochem. Mol. Biol. J. 4, 9. https://doi.org/10.21767/2471-8084.100058

Hu, Q., Xiong, Y., Zhu, G.-H., Zhang, Y.-N., Zhang, Y.-W., Huang, P., Ge, G.-B., 2022. The SARS-CoV-2 main protease (Mpro): Structure, function, and emerging therapies for COVID-19. MedComm 3, e151. https://doi.org/10.1002/mco2.151

Jin, Z., Du, X., Xu, Y., Deng, Y., Liu, M., Zhao, Y., Zhang, B., Li, X., Zhang, L., Peng, C., Duan, Y., Yu, J., Wang, L., Yang, K., Liu, F., Jiang, R., Yang, Xinglou, You, T., Liu, Xiaoce, Yang, Xiuna, Bai, F., Liu, H., Liu, Xiang, Guddat, L.W., Xu, W., Xiao, G., Qin, C., Shi, Z., Jiang, H., Rao, Z., Yang, H., 2020. Structure of Mpro from SARS-CoV-2 and discovery of its inhibitors. Nature 582, 289–293. https://doi.org/10.1038/s41586-020-2223-y

Kamau, S.W., Grimm, F., Hehl, A.B., 2001. Expression of green fluorescent protein as a marker for effects of antileishmanial compounds in vitro. Antimicrob. Agents Chemother. 45, 3654–3656. https://doi.org/10.1128/AAC.45.12.3654-3656.2001

Khalifa, S.A.M., Yosri, N., El-Mallah, M.F., Ghonaim, R., Guo, Z., Musharraf, S.G., Du, M., Khatib, A., Xiao, J., Saeed, A., El-Seedi, H.H.R., Zhao, C., Efferth, T., El-Seedi, H.R., 2021. Screening for natural and derived bio-active compounds in preclinical and clinical studies: One of the frontlines of fighting the coronaviruses pandemic. Phytomedicine Int. J. Phytother. Phytopharm. 85, 153311. https://doi.org/10.1016/j.phymed.2020.153311

Kitamura, N., Sacco, M.D., Ma, C., Hu, Y., Townsend, J.A., Meng, X., Zhang, F., Zhang, X., Ba, M., Szeto, T., Kukuljac, A., Marty, M.T., Schultz, D., Cherry, S., Xiang, Y., Chen, Y., Wang, J., 2022. Expedited Approach toward the Rational Design of Noncovalent SARS-CoV-2 Main Protease Inhibitors. J. Med. Chem. 65, 2848–2865. https://doi.org/10.1021/acs.jmedchem.1c00509

Krishnamoorthy, N., Fakhro, K., 2021. Identification of mutation resistance coldspots for targeting the SARS-CoV2 main protease. IUBMB Life 73, 670–675. https://doi.org/10.1002/iub.2465

Laughery, M.F., Wyrick, J.J., 2019. Simple CRISPR-Cas9 Genome Editing in Saccharomyces cerevisiae. Curr. Protoc. Mol. Biol. 129, e110. https://doi.org/10.1002/cpmb.110

Lee, C.-C., Lin, C.-P., Lee, Y.-L., Wang, G.-C., Cheng, Y.-C., Liu, H.E., 2010. Meisoindigo is a promising agent with in vitro and in vivo activity against human acute myeloid leukemia. Leuk. Lymphoma 51, 897–905. https://doi.org/10.3109/10428191003672115

Li, X., Lidsky, P.V., Xiao, Y., Wu, C.-T., Garcia-Knight, M., Yang, J., Nakayama, T., Nayak, J.V., Jackson, P.K., Andino, R., Shu, X., 2021. Ethacridine inhibits SARS-CoV-2 by inactivating viral particles. PLoS Pathog. 17, e1009898. https://doi.org/10.1371/journal.ppat.1009898

Lin, C.-W., Tsai, F.-J., Tsai, C.-H., Lai, C.-C., Wan, L., Ho, T.-Y., Hsieh, C.-C., Chao, P.-D.L., 2005. Anti-SARS coronavirus 3C-like protease effects of Isatis indigotica root and plant-derived phenolic compounds. Antiviral Res. 68, 36–42. https://doi.org/10.1016/j.antiviral.2005.07.002

Liu, H., Iketani, S., Zask, A., Khanizeman, N., Bednarova, E., Forouhar, F., Fowler, B., Hong, S.J., Mohri, H., Nair, M.S., Huang, Y., Tay, N.E.S., Lee, S., Karan, C., Resnick, S.J., Quinn, C., Li, W., Shion, H., Xia, X., Daniels, J.D., Bartolo-Cruz, M., Farina, M., Rajbhandari, P., Jurtschenko, C., Lauber, M.A., McDonald, T., Stokes, M.E., Hurst, B.L., Rovis, T., Chavez, A., Ho, D.D., Stockwell, B.R., 2022. Development of optimized drug-like small molecule inhibitors of the SARS-CoV-2 3CL protease for treatment of COVID-19. Nat. Commun. 13, 1891. https://doi.org/10.1038/s41467-022-29413-2

Ma, C., Sacco, M.D., Hurst, B., Townsend, J.A., Hu, Y., Szeto, T., Zhang, X., Tarbet, B., Marty, M.T., Chen, Y., Wang, J., 2020. Boceprevir, GC-376, and calpain inhibitors II, XII inhibit SARS-CoV-2 viral replication by targeting the viral main protease. Cell Res. 30, 678–692. https://doi.org/10.1038/s41422-020-0356-z

Peng, B., Williams, T.C., Henry, M., Nielsen, L.K., Vickers, C.E., 2015. Controlling heterologous gene expression in yeast cell factories on different carbon substrates and across the diauxic shift: a comparison of yeast promoter activities. Microb. Cell Factories 14, 91. https://doi.org/10.1186/s12934-015-0278-5

Sandman, K.E., Marla, S.S., Zlokarnik, G., Lippard, S.J., 1999. Rapid fluorescence-based reporter-gene assays to evaluate the cytotoxicity and antitumor drug potential of platinum complexes. Chem. Biol. 6, 541–551. https://doi.org/10.1016/S1074-5521(99)80086-6

Shi, Y., Shuai, L., Wen, Z., Wang, C., Yan, Y., Jiao, Z., Guo, F., Fu, Z.F., Chen, H., Bu, Z., Peng, G., 2021. The preclinical inhibitor GS441524 in combination with GC376 efficaciously inhibited the proliferation of SARS-CoV-2 in the mouse respiratory tract. Emerg. Microbes Infect. 10, 481–492. https://doi.org/10.1080/22221751.2021.1899770

Troiano, G., Nardi, A., 2021. Vaccine hesitancy in the era of COVID-19. Public Health 194, 245–251. https://doi.org/10.1016/j.puhe.2021.02.025

Vázquez-Mendoza, L.H., Mendoza-Figueroa, H.L., García-Vázquez, J.B., Correa-Basurto, J., García-Machorro, J., 2022. In Silico Drug Repositioning to Target the SARS-CoV-2 Main Protease as Covalent Inhibitors Employing a Combined Structure-Based Virtual Screening Strategy of Pharmacophore Models and Covalent Docking. Int. J. Mol. Sci. 23, 3987. https://doi.org/10.3390/ijms23073987

V'kovski, P., Kratzel, A., Steiner, S., Stalder, H., Thiel, V., 2021. Coronavirus biology and replication: implications for SARS-CoV-2. Nat. Rev. Microbiol. 19, 155–170. https://doi.org/10.1038/s41579-020-00468-6

Xue, X., Yang, H., Shen, W., Zhao, Q., Li, J., Yang, K., Chen, C., Jin, Y., Bartlam, M., Rao, Z., 2007. Production of authentic SARS-CoV M(pro) with enhanced activity: application as a novel tag-cleavage endopeptidase for protein overproduction. J. Mol. Biol. 366, 965–975. https://doi.org/10.1016/j.jmb.2006.11.073

Ye, Y., Jin, T., Zhang, X., Zeng, Z., Ye, B., Wang, J., Zhong, Y., Xiong, X., Gu, L., 2019. Meisoindigo Protects Against Focal Cerebral Ischemia-Reperfusion Injury by Inhibiting NLRP3 Inflammasome Activation and Regulating Microglia/Macrophage Polarization via TLR4/NF-κB Signaling Pathway. Front. Cell. Neurosci. 13, 553. https://doi.org/10.3389/fncel.2019.00553

Yuan, M., Huang, D., Lee, C.-C.D., Wu, N.C., Jackson, A.M., Zhu, X., Liu, H., Peng, L., van Gils, M.J., Sanders, R.W., Burton, D.R., Reincke, S.M., Prüss, H., Kreye, J., Nemazee, D., Ward, A.B., Wilson, I.A., 2021. Structural and functional ramifications of antigenic drift in recent SARS-CoV-2 variants. Science 373, 818–823. https://doi.org/10.1126/science.abh1139